ISSN: 1410-8917
Jurnal Kimia Sains & Aplikasi
e-ISSN: 2597-9914

Jurnal Kimia Sains dan Aplikasi 29 (3) (2026): 195-206

Jurnal Kimia Sains dan Aplikasi
Journal of Scientific and Applied Chemistry

Journal homepage: http://ejournal.undip.ac.id/index.php/ksa

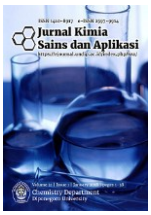

Modification of Polyurethane from Cardanol Biomass of Cashew Nut Shell with Ag Nanoparticles and Its Antibacterial Activity

Magdalena Devi Suryono, Muhammad Ilham Khairuddiin, Fauziyah Azhari, Maulidan Firdaus, Sentot Budi Rahardjo, Witri Wahyu Lestari *

[1] Department of Chemistry, Faculty of Mathematics and Natural Sciences, Universitas Sebelas Maret, Jl. Ir. Surakarta, Central Java 57126, Indonesia

* Corresponding author: witriwahyu@staff.uns.ac.id

https://doi.org/10.14710/jksa.29.3.195-206

Article Info

Article history:

Received: 25th August 2025
Revised: 16th February 2026
Accepted: 26th February 2026
Online: 22nd April 2026

Keywords:
Cardanol; polyol; polyurethane; silver nanoparticles; antibacterial

Abstract

The cardanol-based polyurethane was systematically investigated for its chemical structure, thermal stability, surface hydrophobicity, morphology, dispersion of silver nanoparticles (AgNPs), crystalline features, and antibacterial performance. In this study, a Biobased polyurethane (PU) derived from cardanol extracted from cashew nut shell liquid (CNSL) was modified with silver nanoparticles (AgNPs) to develop antibacterial composite materials. Cardanol was isolated via liquid–liquid extraction and further purified using column chromatography. Fourier Transform Infrared (FTIR) spectroscopy and High-Performance Liquid Chromatography (HPLC) confirmed the successful removal of anacardic acid and the presence of cardanol. The cardanol-based polyol was synthesized via a thiol–ene click reaction and subsequently polymerized with 1,4-butanediol and hexamethylene diisocyanate to produce an elastomeric PU. AgNPs were incorporated at various loadings to evaluate their influence on physicochemical properties and antibacterial activity. FTIR analysis verified urethane bond formation, while thermogravimetric and differential thermal analysis (TG/DTA) demonstrated thermal stability up to 200°C. X-ray Diffraction (XRD) confirmed the face-centered cubic (FCC) crystalline structure of silver within the PU matrix. Field-emission scanning electron microscopy-energy dispersive X-ray (FESEM-EDX) revealed that PU containing 15 wt% AgNPs exhibited the most homogeneous nanoparticle dispersion. An increase in AgNPs content led to enhanced surface hydrophobicity and antibacterial performance. Antibacterial essays showed PU/AgNPs composites effectively inhibited *Escherichia coli* and *Staphylococcus aureus*, with the largest inhibition zones observed for PU/Ag containing 15 wt% AgNPs (16.40 mm and 12.60 mm, respectively). Overall, the results indicated that AgNP loading governs a trade-off between dispersion uniformity and antibacterial efficacy, with intermediate loading favoring homogeneous morphology and higher loading maximizing antibacterial performance. These findings highlight the potential of PU/AgNPs composites for use as antibacterial coating materials.

1. Introduction

Urinary tract infection (UTI) is one of the most common healthcare-associated infections. In Indonesia, the prevalence of UTI is estimated to reach 90–100 cases per 100,000 population per year, equivalent to approximately 180,000 new cases annually [1]. A key risk factor for catheter-associated urinary tract infections (CAUTIs) is prolonged catheterization, which increases the likelihood of bacteriuria by 5–10% per day after insertion, potentially reaching 90–100% in long-term use [2]. The most common causative bacteria include *Escherichia coli* and *Staphylococcus aureus* [3]. From a materials perspective, developing antibacterial polymer coatings derived from renewable resources remains a significant challenge.

To reduce infections from long-term catheter use, there is growing interest in anti-infective catheters, such as those coated with antibacterial agents or silver nanoparticles (AgNPs). Clinical evidence shows that drug-coated catheters (e.g., chlorhexidine-silver sulfadiazine) significantly reduce infection rates [4]. AgNPs are widely applied in antibacterial surfaces due to their broad-spectrum bactericidal activity and have been incorporated into various consumer and medical products [5]. A promising strategy involves embedding AgNPs into polyurethane (PU) matrices. PU is among the six most widely used synthetic polymers and is synthesized from isocyanates, polyols, and diols. Most commercial PUs are derived from petroleum-based polyols, valued for their high hydroxyl content and low acid values [6, 7]. However, these polyols are non-renewable and raise environmental and health concerns due to toxic, carcinogenic intermediates, such as phosgene [8].

As fossil resources become increasingly limited, the development of renewable, bio-based materials for PU synthesis is gaining momentum. Biomass-derived polyols offer environmental benefits and align with green chemistry principles. Various natural resources such as corn, wheat straw, and cashew nut shells are being investigated as alternative feedstocks [9]. Biomass is considered carbon-neutral because it absorbs atmospheric CO_2 during growth and releases it upon degradation, forming a closed carbon cycle [10]. Biomass includes organic material from plants, animals, agricultural residues, industrial waste, algae, and microbial sources, offering diverse chemical functionalities and high availability [11]. The utilization of biomass for polyol and PU production supports sustainable development and circular bioeconomy efforts [9]. Unlike previously reported cardanol-derived PU systems, this work employs thiol–ene click chemistry to enable controlled polyurethane formation and effective incorporation of AgNPs, resulting in enhanced antibacterial performance.

In Indonesia, the cashew tree (*Anacardium occidentale*) is cultivated on a large scale, with a plantation area of over 436,000 hectares. Between 2016 and 2022, its average annual production grew by 3.8% [12]. However, cashew processing generates substantial amounts of cashew nut shell waste, which can cause environmental pollution if not properly managed. This waste can be converted into cashew nut shell liquid (CNSL), a valuable by-product rich in phenolic compounds, including cardanol (60–65%), cardol (15–20%), and minor components such as methyl cardol [13, 14]. Cardanol is the most prominent component and has been recognized as a potential precursor for the synthesis of high-value products, including epoxies, phenolic resins, and polyols. Its chemical structure allows it to be modified into hydroxyl-rich compounds suitable for PU production [15].

Despite extensive studies on PU/AgNP systems, reports on cardanol-based polyurethane matrices modified via click chemistry for antibacterial coating applications remain limited. Therefore, this research proposes the development of PU coatings derived from cardanol biomass extracted from CNSL and modified with AgNPs. This approach offers a dual benefit: preventing catheter-associated infections through antibacterial PU/AgNPs surfaces and promoting the valorization of agricultural waste through the use of renewable biomass The study aims to synthesize and characterize PU-based materials from CNSL-derived polyols and evaluate the effect of AgNPs incorporation on their physicochemical and antibacterial properties, while mechanical and biocompatibility evaluations are beyond the scope of the present work and will be addressed in future studies.

2. Experimental

2.1. Materials

CNSL was provided by Minyak Kulit Mete Indonesia (MKMI) Ltd., Sukoharjo. n-hexane, ethyl acetate, distilled water, and activated carbon were purchased from Agung Jaya. Silica gel 60 (Millipore, 0.063-0.200 mm), methanol (99%), ammonium hydroxide (NH_4OH, 25%), hydrochloric acid (HCl, 37%), anhydrous sodium sulfate (Na_2S_2O4, 82%), 2-mercaptoethanol (99%), Azobisisobutyronitrile (AIBN, 20%), 1,4-butanediol (BDO, 99%), hexamethylene diisocyanate (HMDI, 98%), triethyl amine (TEA, 99%), 1,5,7-triazabicyclo[4.4.0]dec-5-ene (TBD, 98%), and tetrahydrofurane (THF, 99%) were commercially obtained from Sigma Aldrich. Commercial silver nanoparticles (AgNPs) were supplied as a 1 ppm aqueous dispersion with an average particle size of 20–30 nm, stabilized with polyethylene glycol (PEG) according to the manufacturer's specifications, and purchased from Sigma-Aldrich. McFarland Equivalence Turbidity Standards (Lenexa, Kansas, 0.5 MFU), bacteria *Escherichia coli* (Culti-Loops R4607050 ATCC 25922 Remel Europe), bacteria *Staphylococcus aureus* (Culti-Loops R4607010 ATCC 25923 Remel Europe), Chloramphenicol (Oxoid C30 Road Basingstroke 3729036), Mueller-Hinton Agar 500g (Millipore Sigma-Aldrich VM1051772 322 1.03872.0500), Filter paper (Whatman 42).

2.2. Characterization

The pH of the sample was measured at room temperature using a calibrated pH meter (ATC PH=009) by immersing the electrode in the solution until a stable reading was obtained. The viscosity of the environment was evaluated qualitatively by visual observation of the sample's flow behavior: free-flowing behavior indicated low viscosity, and slow or resistant flow indicated higher viscosity. FTIR (Shimadzu tipe IR Prestige-21, 400-4000 cm^{-1}, KBr) was used to analyze the functional group of the materials, HPLC (Waters The Science of What's Possible e2695 with UV Detector Waters 2489 dan Reliant C18 5µm 4.6×150 mm Column) to analyze the component of CNSL, XRD (Expert Pan Analytical, 2θ = 10-90° with Cu detector), thermal stability of the material was measured using TG/DTA (Linseis Simultaneous Thermal Analysis PT 1600, 0–100°C, with heating rate 10°C/minute), FESEM-EDX (Jeol/MP JSM-IT700HR Version 3). Gel Permeation Chromatography (GPC) (TSKgel SuperAW5000, Solvent THF) was used to analyze the molecular weight of PU.

2.3. Experiment

2.3.1. Isolation of Cardanol from CNSL

Cardanol was isolated from technical CNSL by liquid-liquid extraction. Technical CNSL (100 g) was dissolved in methanol (320 mL), followed by the addition of NH_4OH (25%, 200 mL), and stirred using a magnetic stirrer at 300 rpm for 45 minutes. The mixture was then extracted with n-hexane (2 × 200 mL). The organic layer was washed with 5% HCl (100 mL), followed by distilled water (100 mL). Activated charcoal (10 g) was added to the organic layer, and the mixture was stirred at 300 rpm for 45 minutes. The filtrate was dried with anhydrous Na_2SO_4 to obtain pure cardanol [13]. The isolate was then purified by column chromatography using silica gel 60 (0.063–0.200 mm) as the stationary phase and 2×100 mL of n-hexane: ethyl acetate (9:1) as the eluent. The column fractions were grouped based on thin-layer chromatography (TLC) profiles using three eluent systems: n-hexane:ethyl acetate (9:1), n-hexane: chloroform (1:1), and n-hexane:chloroform:ethyl acetate (7:3:1) [16]. The obtained cardanol was then subjected to physicochemical analysis and characterized using FTIR and HPLC. The calculation of cardanol yield is shown in Equation (1).

$$\%\ yield\ of\ cardanol = \frac{mass\ of\ cardanol\ extracted\ (g)}{mass\ of\ CNSL\ (g)} \times 100\% \quad (1)$$

2.3.2. Synthesis of Cardanol-Based Polyol

The synthesis of polyol A based on cardanol was carried out through a thiol-ene reaction. A total of 10 mL (0.03 mol) of cardanol was mixed with 4 mL (0.057 mol) of 2-mercaptoethanol (molar ratio [mercaptoethanol]:[double bond] = 2:1). The mixture was then added with 1–2 mol % of AIBN (0.6 mmol) as a radical initiator, and the reaction was conducted under a nitrogen atmosphere. The mixture was refluxed at a temperature of 60–65°C for 30 minutes. It was then stirred and maintained at 60–65°C for 4.5 hours [17, 18]. The resulting polyol was analyzed for its physical properties and characterized using FTIR. The calculation of polyol yield is shown in Equations (2) and (3) (MW polyol = 318.5 g/mol).

$$Theoretical\ mass\ of\ polyol = (massa\ \times Mr)\ polyol \quad (2)$$

$$\%\ yield\ of\ polyol = \frac{mass\ of\ polyol\ synthesis\ (g)}{Theoretical\ mass\ of\ polyol\ (g)} \times 100\% \quad (3)$$

2.3.3. Synthesis of PU

A total of 0.138 g (1.37 mmol) of BDO and 3.82 g (1.37 mmol) of polyol A were heated to 100°C in a round-bottom flask with a magnetic stirrer. Then, 0.718 g (2.74 mmol) of HMDI was added, followed by 0.179 mmol of TBD catalyst and 0.247 mmol of TEA. The mixture was stirred for 2–3 minutes and then cured in an oven at 100°C for 24 hours to produce PU elastomer. The resulting PU was analyzed for its physical properties, hydrophobicity, and characterized using FTIR, TG/DTA, XRD, GPC, and FE-SEM EDX. In the synthesis of PU elastomers, polyol A and BDO were heated to 100°C to reduce viscosity and ensure homogeneity prior to the addition of HMDI as the diisocyanate component. The calculation of PU yield is shown in Equations (4) and (5).

$$Theoretical\ mass\ of\ PU = mass\ of\ BDO + mass\ of\ polyol + mass\ of\ HMDI \quad (4)$$

$$\%\ yield\ of\ PU = \frac{mass\ of\ PU\ synthesis\ (g)}{Theoretical\ mass\ of\ PU\ (g)} \times 100\% \quad (5)$$

2.3.4. Modification of PU with AgNPs and Their Variation

A total of 0.5 g of PU was dissolved in 5 mL of THF to form a coating solution, then poured into a petri dish and added with AgNPs in variations: 5% (w/w) PU, 10% (w/w) PU, and 15% (w/w) PU. The mixture was then dried at room temperature for 24 hours. PU/AgNPs were analyzed for their physical properties, hydrophobicity, and characterized using FTIR, XRD, FE-SEM EDX, and antibacterial activity tests.

2.3.5. Contact Angle Testing of PU (0% w/w) and Variation PU/Ag

Contact angle testing was conducted to evaluate the surface wettability of cardanol-based PU samples using the static drop method. The molded and dried PU samples were placed on a clean, flat surface. Next, a drop of distilled water (approximately 3–5 µL) was slowly dropped onto the sample surface using a micropipette or syringe. After the drop stabilized, an image of the drop was captured using a camera or a contact angle measuring system integrated with analysis software. The contact angle was measured between the tangential lines at the meeting points between the solid, liquid, and air surfaces. This test was conducted at room temperature with measurements at a minimum of three different points on the sample surface to obtain a representative average value of the PFPU contact angle. Modification with PFPU successfully increased the contact angle of the material, making it more hydrophobic [5]. This analysis used water droplets with three repetitions and was assisted by ImageJ software.

2.3.6. Antibacterial Activity Testing of PU/AgNPs

The test began with sterilizing glassware in an autoclave at 170°C for 2 hours. Agar media was prepared by mixing 0.76 g of Mueller Hinton Agar (MHA) with 120 mL of distilled water and sterilized at 121°C under 2 atm pressure for 2 hours to produce agar media in petri dishes. Bacterial suspensions of *Staphylococcus aureus* ATCC 25923 and *Escherichia coli* ATCC 25922 were spread onto the agar media. Holes were made in the agar using a cork borer, and the wells were filled with samples: PU, PU/Ag (5%w/w), PU/Ag (10% w/w), and PU/Ag (15% w/w), with chloramphenicol as a positive control and THF as a negative control. The plates were then incubated at 37°C for 24 hours. Inhibition zones were measured using a caliper. The well diffusion assay was used as a preliminary qualitative method to compare antibacterial activity; however, its limitations for solid polymer films are acknowledged.

3. Results and Discussion

3.1. Isolation of Cardanol from CNSL

Cardanol was isolated from technical CNSL using a liquid–liquid extraction method. Preliminary purification was performed by adding activated charcoal

to adsorb colored and polar impurities, followed by filtration and drying with anhydrous Na_2SO_4, which was used as a drying agent to remove residual moisture from the organic phase. Further purification was conducted by column chromatography using silica gel 60 as the stationary phase to separate components based on differences in polarity, with *n*-hexane: chloroform: ethyl acetate (7:3:1, v/v), *n*-hexane: ethyl acetate (9:1, v/v), and *n*-hexane: chloroform (1:1, v/v) as the eluent. The resulting fractions were combined based on their TLC profiles. The TLC analysis of the purified fraction showed a single spot, indicating successful isolation of cardanol, as presented in Figure 1.

The TLC results revealed five fractions, with the third fraction showing a single spot, indicating the possibility of a pure isolate. Purity testing was conducted using three different eluent systems, yielding R_f values of 0.625, 0.7, and 0.75, respectively. The isolated cardanol exhibited different physical properties compared to CNSL, as shown in Table 1.

The isolation of cardanol from CNSL showed good results, as evidenced by a pH change from 5 to 7, indicating successful purification and reduced acidic compounds. The color of cardanol changed from dark brown to reddish brown (Figure 2), consistent with the references [13]. The density also closely matched the reference value, with the isolated cardanol having a density of 0.932 g/cm^3 compared to the standard 0.92 g/cm^3.

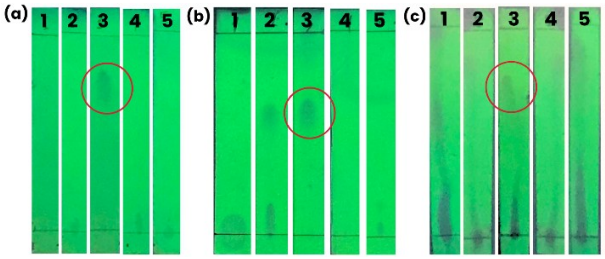

Figure 1. TLC results profile in different solvent mixture as eluent: (a) *n*-hexane: chloroform: ethyl acetate (7:3:1 left); (b) *n*-hexane: ethyl acetate (9:1, middle); (c) *n*- hexane: chloroform (1:1, right)

Table 1. Results of analysis of the physical and chemical properties of cardanol from CNSL

Characteristic	Obtained from experiment	References
pH CNSL	4.70	4.97 [13]
pH cardanol	6.50	6.80 [13]
Color of CNSL	Dark brown	Dark brown [13]
Color of cardanol	Reddish brown	Reddish brown [13]
Mass density of CNSL	0.974 g/cm^3	0.973 g/cm^3 [19]
Mass density of cardanol	0.932 g/cm^3	0.920 g/cm^3 (ISO 12185)
Yield of cardanol	25.6%	28.64% [20]

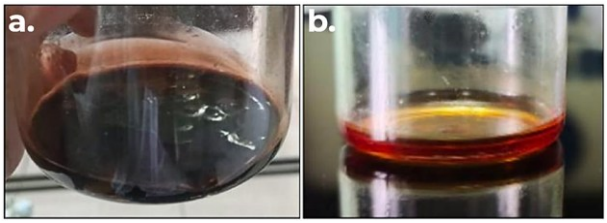

Figure 2. Visual comparison of CNSL color with isolated cardanol: (a) CNSL and (b) cardanol

3.2. Synthesis of Cardanol-Based Polyol

Polyol was synthesized from cardanol through a thiol-ene reaction between the thiol group (−SH) of 2-mercaptoethanol and the double bond on the alkyl chain of cardanol, using AIBN as a free radical initiator. The differences in physical properties between cardanol and polyol A are shown in Table 2.

The data in Table 2 show that the physical and chemical properties of cardanol changed after being modified into a polyol. The color shifted from reddish brown to clear yellowish (Figure 3), indicating a reduction in double bonds and conjugation due to the thiol-ene reaction, resulting in a lighter-colored solution [21]. The viscosity of the polyol decreased significantly compared to cardanol due to the introduction of hydroxyl groups, which increased its polarity and flexibility [17]. This facilitates better mixing in subsequent reactions, such as PU formation.

Cardanol has high viscosity due to strong Van der Waals interactions from its aromatic structure and long alkyl chain. After being modified into a polyol, the addition of hydroxyl groups increases the molecule's polarity and flexibility, leading to a significant reduction in viscosity (Figure 3). This low viscosity facilitates downstream processes such as PU synthesis. The polyol synthesis demonstrated high efficiency with a yield of up to 90%, confirming the successful thiol-ene reaction between cardanol and 2-mercaptoethanol, as illustrated in the reaction scheme in Figure 4.

Table 2. Physical and chemical properties of polyol derived from cardanol

Characteristic	Polyol	Cardanol
Color	Clear yellowish	Reddish brown
Viscosity	Low (fluid)	High (oily)

Figure 3. Synthesized polyol from cardanol

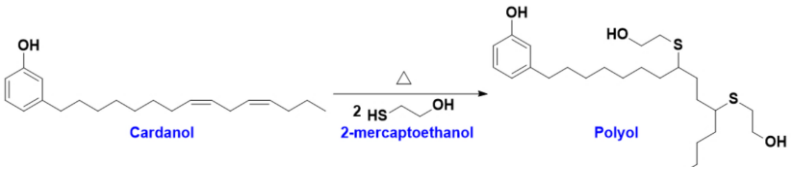

Figure 4. Synthesis reaction of polyol-based cardanol (modified from reference [17])

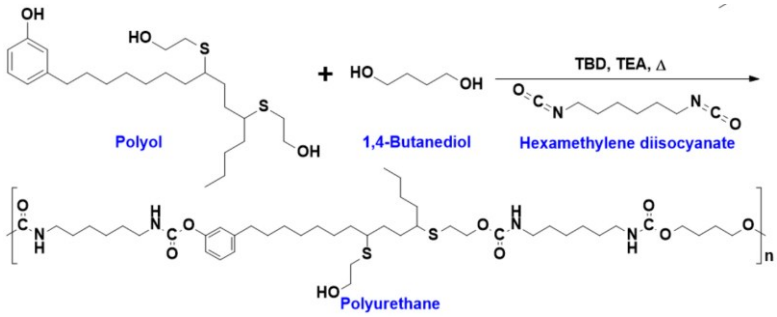

Figure 5. Reaction scheme in the synthesis of polyurethane (modified from reference [22])

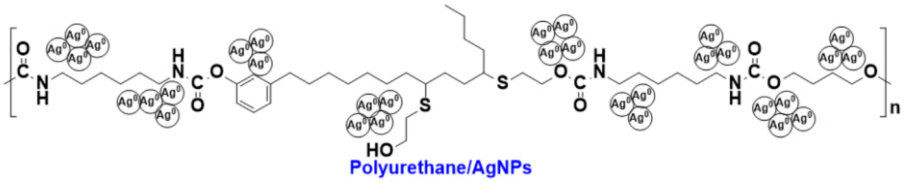

Figure 6. Schematic of PU/AgNPs composite formation (modified from reference [22])

3.3. Synthesis of PU

As shown in Figure 5, polyol acts as the soft segment of the PU, while BDO acts as the hard segment. This reaction falls under the category of typical PU synthesis reactions commonly used to produce elastomeric materials. HMDI forms urethane bonds with –OH groups, contributing to mechanical flexibility. Catalysts TBD and TEA were added to accelerate the reaction and improve conversion efficiency. Resulting in a white PU elastomer with a crosslinked structure formed by the reaction between isocyanate and hydroxyl groups. This crosslinking produced a material that is both flexible and durable. The physical properties of the synthesized PU are summarized in Table 3.

Based on Table 3, the synthesized PU exhibits a pale yellowish-white color and an elastomeric form, consistent with the typical characteristics of PU reported in the literature. These attributes indicate that the reaction proceeded successfully and the flexible polymer structure was effectively formed. The synthesis yield reached 99% (based on Equations (4) and (5)), indicating high efficiency and suggesting that the reaction proceeded almost completely under the optimized conditions, temperature (100°C), and time (2–3 minutes).

Table 3. Physical properties of the synthesized PU

Characteristic	This study	Literature reference
Colour	Pale yellowish white	Pale yellowish white [23]
Form	Elastomer	Foam, elastomer, or solid [24]

3.4. Modification of PU with the Addition of AgNPs and Their Variations

AgNPs were incorporated into the PU matrix to enhance its antibacterial properties and hydrophobicity. As illustrated in Figure 6, AgNPs interact physically, not chemically, with the PU chains, primarily through adsorption into polar groups. This interaction helps maintain a stable, uniform distribution of AgNPs within the matrix, thereby improving antibacterial activity. This method yields a flexible PU/AgNPs composite suitable for medical applications.

The hydrophobicity of PU, both with and without AgNPs incorporation, was evaluated using a contact angle measurement test. A larger contact angle indicates a higher degree of hydrophobicity. The results of the contact angle measurements are shown in Figure 7.

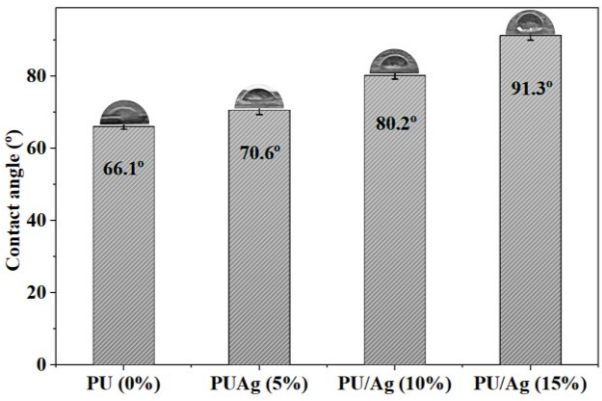

Figure 7. Bar chart of contact angle analysis for PU (0% w/w), PU/Ag (5% w/w), PU/Ag (10% w/w), and PU/Ag (15% w/w)

As shown in Figure 7, the addition of AgNPs to PU significantly increased hydrophobicity, evidenced by the rise in contact angle from 66.1° (pure PU) to 91.3° (PU/Ag (15% w/w)). This improvement is attributed to changes in surface morphology and roughness introduced by the presence of AgNPs, which reduce water interaction with the surface. The higher the AgNP concentration, the greater the observed hydrophobic effect.

3.5. Characterization Analysis of PU with the Addition of AgNPs and Their Variations

3.5.1. FTIR Analysis

CNSL contains several major compounds: cardanol, cardol, anacardic acid, and 2-methylcardol, with cardanol being the predominant component. Cardanol possesses an unsaturated hydroxyl group, an aromatic ring, and a hydrophobic alkyl chain, making it a promising renewable material for polymer production [17]. FTIR characterization results of CNSL, cardanol, polyol, PU, and PU/Ag are presented in Figure 8 and Table 4. The FTIR spectrum of CNSL shows a strong absorption band at 3553 cm^{-1}, characteristic of a free hydroxyl (−OH) group, consistent with the report by Rahmawati *et al.* [13]. After isolation, this band shifted to 3425 cm^{-1} in the cardanol spectrum, suggesting the −OH group remains present but in a different chemical environment. Additionally, the CNSL spectrum shows a peak at 2363 cm^{-1}, corresponding to the aromatic C=O stretch of the carboxylic acid group (−COOH) in anacardic acid. The disappearance of this peak in the cardanol spectrum confirms the removal of the acid fraction and successful isolation of cardanol.

Other key absorptions present in both CNSL and cardanol include aromatic C−H (3008−3011 cm^{-1}), aliphatic C−H (2924−2928 cm^{-1}), and aromatic C=C (1576−1599 cm^{-1}), indicating the presence of an aromatic ring with an unsaturated aliphatic chain — a defining structural feature of CNSL and its derivatives. The phenolic C−O stretch was also detected at 1089 cm^{-1} in CNSL and shifted to 1110 cm^{-1} in cardanol, confirming the presence of active phenolic groups [16]. The polyol spectrum revealed several notable changes. The O−H stretching band shifted to 3333 cm^{-1}, indicating a new hydroxyl environment, possibly due to intra/intermolecular interactions or the introduction of other groups (e.g., −SH). A new absorption band at 1167 cm^{-1}, absent in both CNSL and cardanol, was assigned to aliphatic C−O stretching, confirming the success of chemical modification [25]. Additionally, a −C−S stretching band at 633 cm^{-1} indicates the successful incorporation of thiol groups from 2-mercaptoethanol [26].

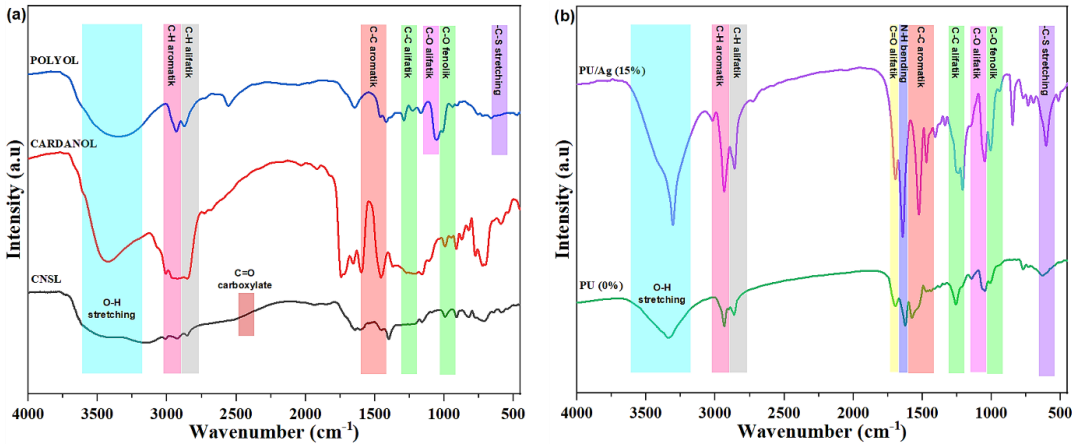

Figure 8. FTIR spectra of (a) CNSL, cardanol, and polyol and (b) PU and PU/Ag (15% w/w)

Table 4. List of observed peaks of FTIR spectra of CNSL, cardanol, polyol, PU, and PU/Ag (15% w/w) compared to literature references

Bonding type	CNSL	Cardanol	Polyol	PU	PU/Ag	Ref.
O−H stretching	3553	3425	3333	3340	3306	[13]
C−H aromatic	3011	3008	3000	3004	3019	[16]
C−H aliphatic	2928	2924	2931	2933	2934	
C=O aromatic (carboxylic acid)	2363	-	-	-	-	[13]
C=O aliphatic	-	-	-	1696	1695	[19]
N−H bending	-	-	-	1624	1642	[27]
C=C aromatic	1576	1599	1546	1575	1525	[16]
C=C aliphatic	1399	1455	1460	1485	1470	
C-O aliphatic	-	-	1167	1257	1209	[25]
C−O phenolic	1089	1110	1055	1010	1007	[16]
−C−S stretching	-	-	633	630	604	[26]

In both PU and PU/Ag composites, the O–H band shifted further to 3340 cm^{-1} (PU) and 3306 cm^{-1} (PU/Ag), with a notable decrease in intensity. This suggests a reaction between the hydroxyl groups of the polyol and the isocyanate groups, leading to urethane bond formation. New absorption bands appeared at 1696 cm^{-1} (PU) and 1695 cm^{-1} (PU/Ag), corresponding to the aliphatic C=O stretch of urethane linkages [19]. Stronger aliphatic C–O stretching was also observed at 1257 cm^{-1} (PU) and 1209 cm^{-1} (PU/Ag), which were absent in the CNSL and cardanol spectra. Furthermore, N–H bending bands at 1624 cm^{-1} (PU) and 1642 cm^{-1} (PU/Ag) are characteristic of urethane groups [27]. The aromatic C=C band remained detectable within the 1525–1575 cm^{-1} range, indicating the phenolic structure of cardanol was preserved in the final PU structure. The phenolic C–O stretch shifted to lower wavenumbers at 1010 cm^{-1} (PU) and 1007 cm^{-1} (PU/Ag), suggesting a change in the chemical environment due to new structural formation. The –C–S stretching band remained visible at 630 cm^{-1} (PU) and 604 cm^{-1} (PU/Ag), indicating the thiol group remained incorporated within the modified PU structure.

3.5.2. HPLC Characterization of Cardanol from CNSL

HPLC analysis was performed to identify the major compounds in cardanol isolated from CNSL and compare them with published data. HPLC was employed as a qualitative technique to confirm the presence of cardanol, while quantitative purity determination was not performed due to the absence of certified calibration standards. The chromatogram is shown in Figure 9.

The red and blue lines represent CNSL and isolated cardanol, respectively. The CNSL chromatogram exhibited major peaks at 6.114, 8.436, 12.995, 14.747, and 21.567 minutes, which are comparable to reported retention times [28] (6.851, 9.664, 15.528, and 22.938 minutes). The isolated cardanol chromatogram showed peaks at 2.246, 4.796, and 10.661 minutes. Based on Phani Kumar *et al.* [29], these peaks can be assigned to trienic cardol (~3.8 minutes; 8Z,11Z,14-pentadecatrienyl), dienic cardol (~4.3 minutes), and dienic cardanol (~10 minutes; 8Z,11Z-pentadecadienyl), respectively. The presence of cardol in the isolated product likely arises from incomplete separation during the isolation process, possibly influenced by variations in temperature or reaction time. Although cardol was not the intended target, its presence does not hinder PU synthesis due to the high reactivity of its phenolic groups. Nevertheless, further purification is recommended to reduce cardol content and ensure that the final PU product achieves optimal physical and chemical properties for coating applications.

3.5.3. GPC Characterization of Synthesized PU

The synthesized PU was characterized by GPC to evaluate its molecular weight distribution and polydispersity index (PDI), as shown in Figure 10. THF was used as the solvent due to its good solubility for polyurethane and compatibility with the chromatographic system and detector. The chromatogram displayed two distinct peaks, indicating the presence of different molecular-weight fractions. Peak 1, representing 18.6% of the total area, was attributed to the PU fraction, with a weight-average molecular weight (Mw) of 1,789 g/mol, number-average molecular weight (Mn) of 442 g/mol, and peak molecular weight (Mp) of 970 g/mol. The PDI of 1.13 suggests a relatively broad molecular weight distribution, which is typical for step-growth polymerization systems such as polyurethane synthesis.

In contrast, Peak 2, comprising 81.4% of the area, showed an extremely low molecular weight (MW = 1948, Mn = 7176, and Mz = 3.68 g/mol). This suggests the presence of unreacted monomers, residual solvents, or low-molecular-weight oligomers. Given its minimal molecular weight and lack of polymeric characteristics, Peak 2 was excluded from further analysis as it does not represent the actual polymer product. Although Peak 1 represents a smaller proportion of the total chromatogram area, it is the most relevant for evaluating the success of the PU synthesis, as it reflects the fraction of material that underwent successful polymerization and formed the intended PU structure.

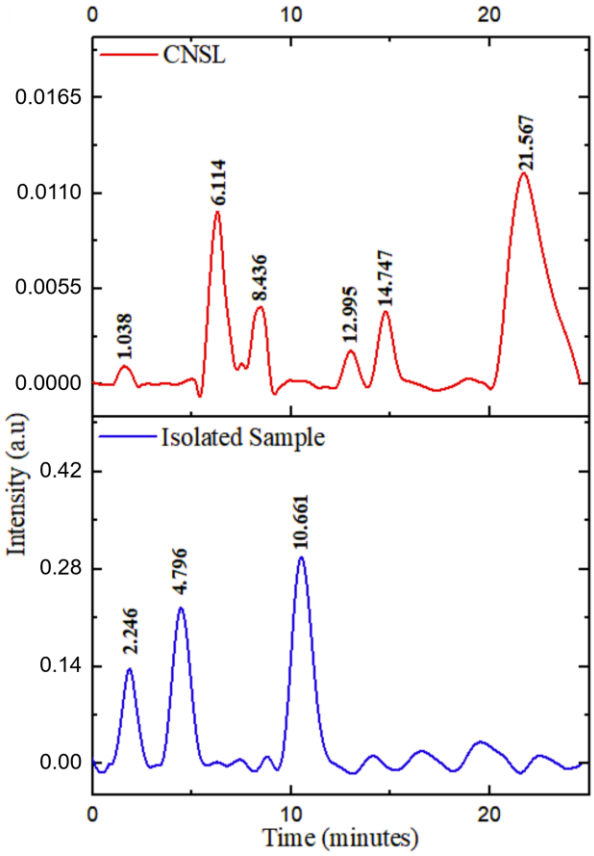

Figure 9. HPLC chromatogram of CNSL and cardanol samples using an acetonitrile:water:formic acid (60:20:20) eluent, at a flow rate of 1.80 mL/min and detection at 280 nm

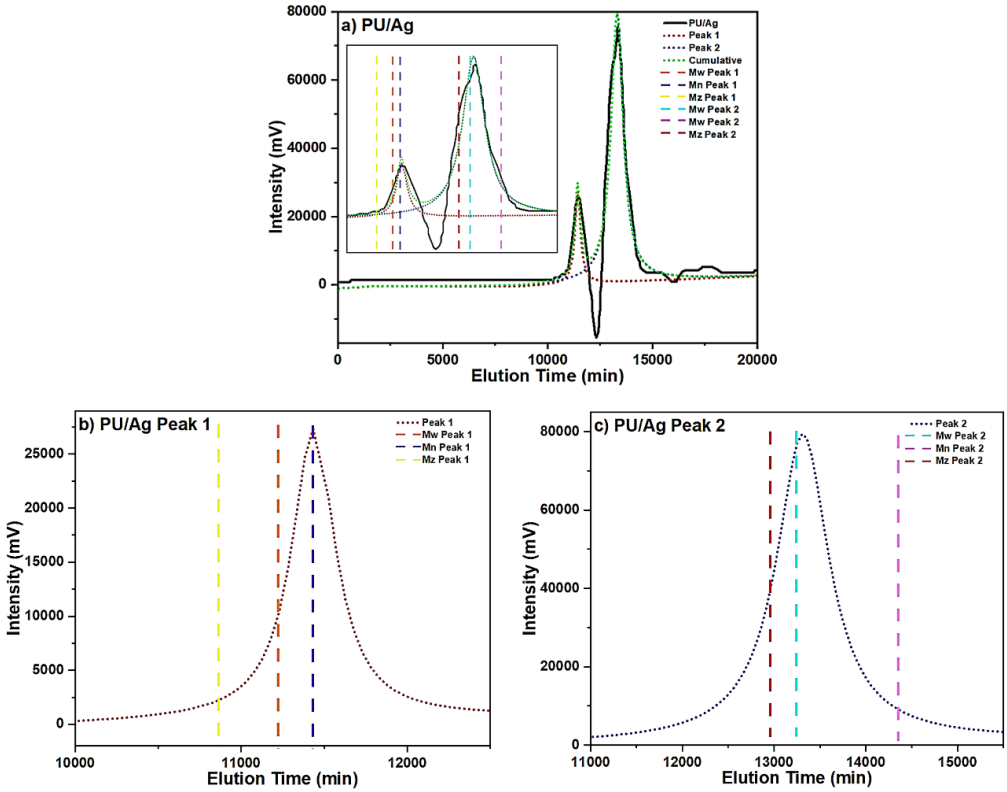

Figure 10. GPC chromatogram of (a) deconvolution, (b) peak, and (c) peak 2 1 the PU sample

Compared to the data reported by Bramhecha and Sheikh [30], in which the synthesized PU had an Mn of 64,645 Da, MW of 82,074 Da, and a PDI of 1.269, indicating a relatively uniform chain length, the PU synthesized from cardanol in this study exhibited a significantly broader molecular weight distribution. This difference may be attributed to the inherent reactivity of cardanol, suboptimal reaction conditions, or the lack of additional purification steps. The progress of the thiol–ene reaction was inferred from characteristic FTIR spectral changes; however, the extent of conversion was not quantitatively confirmed by NMR analysis, and therefore, complete conversion is not claimed. The relatively low molecular weight of the synthesized PU may be attributed to the cardanol-based polyol structure, the thiol–ene modification, and possible chain-termination effects during polymerization. Therefore, direct comparison with petroleum-based PU systems reported in the literature should be made with caution. A PDI value of 4.050 indicates substantial chain length variability, which may affect the physical properties and overall performance of the PU in its intended applications [31].

3.5.4. TG-DTA Analysis

The thermal stability of cardanol-based PU films is shown in Figure 11. Based on thermal analysis, the PU exhibits a characteristic two-step degradation pattern, consistent with previous findings [18]. These two stages reflect the primary mechanisms of PU decomposition, strongly influenced by the chemical composition and polymer structure derived from cardanol-based synthesis.

The thermal degradation of cardanol-based PU films occurs in two main stages (Figure 11). The first stage (200–400°C, 46.99%) corresponds to the breakdown of urethane groups, while the second stage (400–500°C, 50.42%) involves the degradation of the polymer backbone. The DTA curve displays two exothermic peaks without any prior phase transition, indicating a stepwise degradation accompanied by heat release. The aromatic ring structure in cardanol contributes to the thermal stability of the PU, although the degradation pattern remains typical of PU.

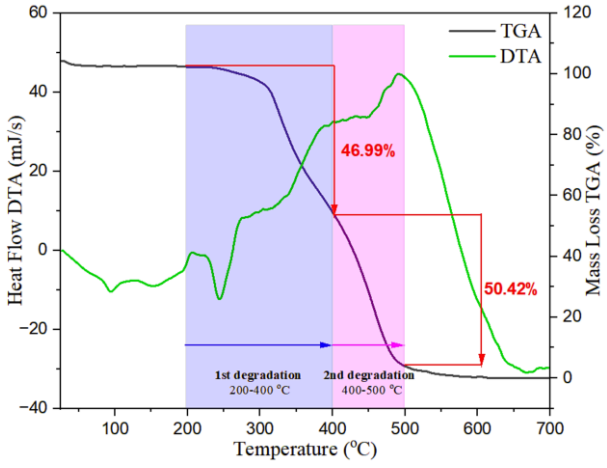

Figure 11. TGA curve of cardanol-based PU

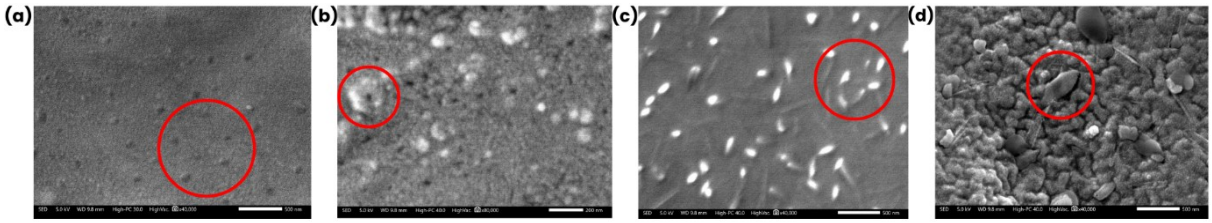

Figure 12. FESEM images of (a) PU, (b) PU/Ag (5% w/w), (c) PU/Ag (10% w/w), and (d) PU/Ag (15% w/w) samples

3.5.5. FESEM-EDX Analysis

The surface characterization results of PU, PU/Ag (5% w/w), PU/Ag (10% w/w), and PU/Ag (15% w/w) samples using FESEM are presented in Figure 12. FESEM analysis of pure PU reveals a smooth, dense, and homogeneous morphology with no bright particles, indicating the absence of metallic nanoparticles. In contrast, PU/Ag (5% w/w) exhibits a rough, layered surface with uniformly dispersed Ag nanoparticles and no signs of agglomeration, suggesting successful blending and potential enhancement of mechanical and antibacterial properties.

In the PU/Ag (10% w/w) sample, AgNPs appear as evenly distributed, spherical-to-oval shapes, further supporting their antibacterial functionality and biomedical potential. PU/Ag (15 % w/w) shows a rougher surface with noticeable protrusions and early signs of nanoparticle agglomeration, which may negatively affect performance. Therefore, the Ag concentration must be carefully controlled to ensure uniform nanoparticle distribution. The EDX mapping results of the three Ag-containing samples are presented in Table 6.

The EDX data (Table 6) show that all samples contain the main PU elements (C, O, S, and N), while Ag is detected from PU/Ag (5% w/w) (0.04%) to PU/Ag (15% w/w) (0.25%), confirming the successful incorporation of AgNPs. The fluctuation in oxygen content, particularly its decrease in PU/Ag (10% w/w), suggests possible physical (non-covalent) interactions between PU's carbonyl groups and the Ag^0 surface. Variations in sulfur content may reflect changes in functional structure, while the increase in carbon and nitrogen levels indicates the dominance of hydrocarbon segments and urethane groups, as well as potential residual $AgNO_3$ precursors.

Table 6. EDX elemental analysis of C, O, S, N, and Ag in PU, PU/Ag5%, PU/Ag10%, and PU/Ag15% samples

Sample	C (%)	O (%)	S (%)	N (%)	Ag (%)
PU	64.77	15.55	12.01	7.67	-
PU/Ag5%	63.57	17.42	9.01	9.96	0.04
PU/Ag10%	70.37	4.85	13.98	10.68	0.12
PU/Ag15%	62.31	19.73	7.20	10.02	0.25

The Ag content detected by EDX was lower than the nominal AgNP loading because EDX is a surface-sensitive and semi-quantitative technique, whereas the AgNP content was calculated based on the bulk formulation (w/w). Therefore, the EDX results represent localized surface detection rather than the total silver content in the PU matrix. Overall, these findings confirm the successful formation of PU/Ag (15% w/w) and highlight changes in surface composition that may influence the material's functional properties.

3.5.6. XRD Analysis

XRD analysis was conducted to identify the crystalline phases in PU (0% w/w) and PU/Ag (15% w/w) samples. PU/Ag (15% w/w) was selected as a representative sample for XRD analysis because it exhibits the highest AgNP loading and the most pronounced antibacterial performance among the investigated formulations. Specific diffraction peaks observed only in the PU/Ag15% sample indicate the presence of AgNPs. The diffraction pattern corresponds to the standard JCPDS file 04-0783, confirming that the AgNPs exhibit a face-centered cubic (FCC) crystal structure. The complete results are presented in Figure 13.

The XRD data show prominent diffraction peaks at approximately 36.18°, 48.53°, 64.24°, and 77.12° in the PU/Ag15% sample, indicating the presence of crystalline silver within the PU matrix. These angles closely align with those reported by Khwanmuang *et al.* [25] for the (111), (200), (220), and (311) crystal planes of FCC silver, which are 36.91°, 48.53°, 60.2°, and 77.06°.

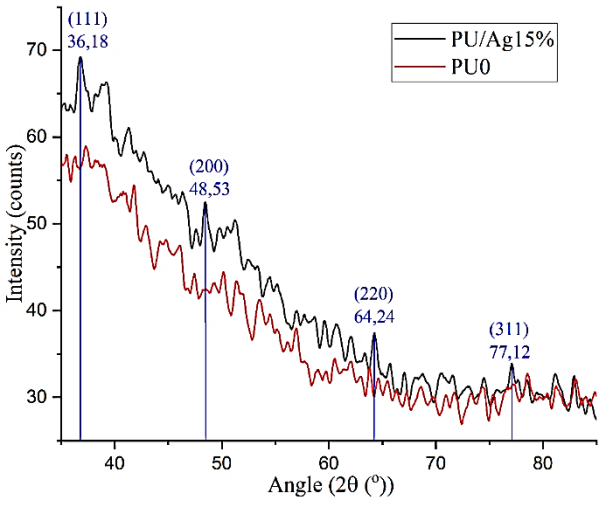

Figure 13. X-ray diffractogram of PU and PU/Ag15% samples

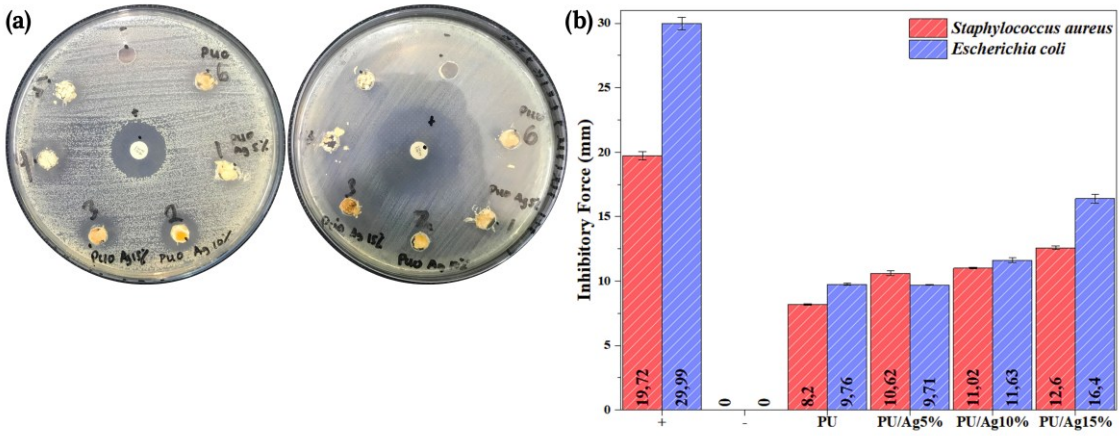

Figure 14. (a) Antibacterial activity test results of chloramphenicol (positive control), THF (negative control), PU (0% w/w), PU/Ag (5% w/w), PU/Ag (10% w/w), and PU/Ag (15% w/w) against *Staphylococcus aureus* and *Escherichia coli*, (b) the histogram of antibacterial activity test results

3.5.7. Antibacterial Test

The antibacterial test results are presented in Figure 14a, with a summary in the histogram shown in Figure 14b. The findings demonstrated that both PU and variation of PU/Ag samples exhibit antibacterial activity against the gram-positive bacterium *Staphylococcus aureus* and the gram-negative bacterium *Escherichia coli.* The enhanced antibacterial performance is attributed to the antibacterial properties of AgNPs, which act through multiple mechanisms, including penetration of the bacterial cell membrane, disruption of protein and DNA structures, and the generation of free radicals that induce oxidative stress in bacterial cells [32]. The effectiveness of AgNPs in the PU system is also influenced by the uniformity of nanoparticle dispersion and the bonding within the polymer matrix.

The control test results showed that the positive control, chloramphenicol, produced inhibition zones with diameters of 19.72 mm against *Staphylococcus aureus* and 29.99 mm against *Escherichia coli*, indicating strong antibacterial activity. In contrast, the negative control, THF, did not show an inhibition zone (0 mm), indicating no antibacterial activity. The PU sample without AgNPs (PU (0% w/w)) exhibited inhibition zones of 8.20 mm against *Staphylococcus aureus* and 9.76 mm against *Escherichia coli*, indicating minimal inherent antibacterial activity of the PU matrix. However, after AgNPs modification, a concentration-dependent increase in antibacterial activity was observed. At 5% AgNPs loading (PU/Ag (5% w/w)), inhibition zones increased to 10.62 mm for *Staphylococcus aureus* and 9.71 mm for *Escherichia coli.* With 10% AgNPs (PU/Ag (10% w/w)), the inhibition zones reached 11.02 mm for *Staphylococcus aureus* and 11.63 mm for *Escherichia coli.* The highest activity was observed in the PU/Ag (15% w/w) sample, which showed inhibition zones of 12.60 mm and 16.40 mm for *Staphylococcus aureus* and *Escherichia coli,* respectively [32].

4. Conclusion

Cardanol was successfully isolated from CNSL with a yield of 25.6%, as confirmed by TLC, FTIR, and HPLC analyses. The cardanol-derived polyol was subsequently used to synthesize PU/AgNP composites with high yield and elastomeric characteristics. The incorporation of AgNPs improved hydrophobicity and thermal stability, while morphological analysis indicated good nanoparticle dispersion at moderate loadings and slight agglomeration at higher AgNP contents. PU/AgNP composites exhibited antibacterial activity against *Escherichia coli* and *Staphylococcus aureus*, with PU/Ag (15% w/w) showing the highest inhibition among the tested formulations. This study was limited to material synthesis, physicochemical characterization, and qualitative antibacterial evaluation; mechanical properties, biocompatibility, and long-term performance were not investigated. Overall, the synthesized PU/AgNP systems demonstrate promising antibacterial properties and may be considered as potential materials for catheter coating applications, pending further mechanical and biocompatibility evaluation.

Acknowledgement

The authors would like to thank BELMAWA DIKTI through the Student Creativity Program (PKM-RE scheme) and LPPM UNS through the Research Group Strengthening Program (PKGR) 2025, Project number 371/UN27.22/PT.01.03/2025, for funding and supporting this research.

References

[1] Waluyo Waluyo, Kusnanto Kusnanto, Yanis %J Jurnal Penelitian Kesehatan" SUARA FORIKES" Kartini, Pencegahan Catheter Associated Urinary Tractus Infection Melalui Catheter Maintenance, *Jurnal Penelitian Kesehatan SUARA FORIKES*, 11, 3, (2020), 291-294 http://dx.doi.org/10.33846/sf11314

[2] Indra Kumala, Nia Triswanti, Hidayat Hidayat, Gilang Raka Pratama, Hubungan Antara Lama Hari Kateter Terpasang dengan Kejadian ISK pada Pasien yang Terpasang Kateter di Ruang Rawat Inap Penyakit Dalam RSUD Dr. H. Abdul Moeloek Provinsi Lampung, *Jurnal Medika Malahayati*, 6, 4, (2021), 239-247

[3] BaiqIsti Hijriani, Manik Retno Wahyunitisari, Agung Dwi Wahyu Widodo, Analysis of *Staphylococcus aureus* and *Escherichia coli* and its Susceptibility to Antibiotic in Catheter-Associated Urinary Tract

Infection Patients at Hospital in Province of West Nusa Tenggara, *Indian Journal of Forensic Medicine & Toxicology*, 16, 2, (2022), 166-173 https://doi.org/10.37506/ijfmt.v16i2.17945

[4] Katherine Belfield, Xinyong Chen, Emily F. Smith, Waheed Ashraf, Roger Bayston, An antimicrobial impregnated urinary catheter that reduces mineral encrustation and prevents colonisation by multi-drug resistant organisms for up to 12 weeks, *Acta Biomaterialia*, 90, (2019), 157-168 https://doi.org/10.1016/j.actbio.2019.03.042

[5] Lirong Wang, Deniz E. Erişen, Ke Yang, Bingchun Zhang, Hongyu Guan, Shanshan Chen, Anticoagulation and antibacterial functional coating on vascular implant interventional medical catheter, *Journal of Biomedical Materials Research Part B: Applied Biomaterials*, 108, 7, (2020), 2868-2877 https://doi.org/10.1002/jbm.b.34618

[6] Indrajeet Singh, Sushanta K. Samal, Smita Mohanty, Sanjay K. Nayak, Recent Advancement in Plant Oil Derived Polyol-Based Polyurethane Foam for Future Perspective: A Review, *European Journal of Lipid Science and Technology*, 122, 3, (2020), 1900225 https://doi.org/10.1002/ejlt.201900225

[7] Yufeng Ma, Yanan Xiao, Yaoli Zhao, Yu Bei, Lihong Hu, Yonghong Zhou, Puyou Jia, Biomass based polyols and biomass based polyurethane materials as a route towards sustainability, *Reactive and Functional Polymers*, 175, (2022), 105285 https://doi.org/10.1016/j.reactfunctpolym.2022.105285

[8] Chao Liang, Ulises R. Gracida-Alvarez, Ethan T. Gallant, Paul A. Gillis, Yuri A. Marques, Graham P. Abramo, Troy R. Hawkins, Jennifer B. Dunn, Material Flows of Polyurethane in the United States, *Environmental Science & Technology*, 55, 20, (2021), 14215-14224 https://doi.org/10.1021/acs.est.1c03654

[9] My Ha Tran, Eun Yeol Lee, Production of polyols and polyurethane from biomass: a review, *Environmental Chemistry Letters*, 21, 4, (2023), 2199-2223 http://dx.doi.org/10.1007/s10311-023-01592-4

[10] Shusheng Pang, Advances in thermochemical conversion of woody biomass to energy, fuels and chemicals, *Biotechnology Advances*, 37, 4, (2019), 589-597 https://doi.org/10.1016/j.biotechadv.2018.11.004

[11] Ahmed I. Osman, Lin Chen, Mingyu Yang, Goodluck Msigwa, Mohamed Farghali, Samer Fawzy, David W. Rooney, Pow-Seng Yap, Cost, environmental impact, and resilience of renewable energy under a changing climate: a review, *Environmental Chemistry Letters*, 21, 2, (2023), 741-764 https://doi.org/10.1007/s10311-022-01532-8

[12] Direktorat Jendral Perkebunan, *Statistik Perkebunan Unggulan Nasional 2020–2022*, Sekretariat Direktorat Jenderal Perkebunan, Jakarta, 2022,

[13] Putri Rahmawati, Ari Handono Ramelan, Soerya Dewi Marliyana, Neng Sri Suharty, Sayekti Wahyuningsih, Synthesis of Cardanol-Based Novolac Resin from Cashew Nut Shell Liquid, *Journal of Engineering Science*, 15, (2019), 23-33 https://doi.org/10.21315/jes2019.15.3

[14] E. B. Mubofu, J. E. Mgaya, Chemical Valorization of Cashew Nut Shell Waste, *Topics in Current Chemistry*, 376, 2, (2018), 8 https://doi.org/10.1007/s41061-017-0177-9

[15] Dinesh Balgude, Anagha Sabnis, Swapan K. Ghosh, Synthesis and characterization of cardanol based aqueous 2K polyurethane coatings, *European Polymer Journal*, 85, (2016), 620-634 https://doi.org/10.1016/j.eurpolymj.2016.03.042

[16] Surya Dewi Marliyana, Sayekti Wahyuningsih, Nisa Nur Hayati, Synthesis of Cardanol-Based Acetaldehyde Novolac Resin from Cashew Nut Shell Liquid (CNSL), *Jurnal Kimia Sains dan Aplikasi*, 25, 9, (2022), 316-321 https://doi.org/10.14710/jksa.25.9.316-321

[17] Maha L. Shrestha, Mihail Ionescu, Xianmei Wan, Nikola Bilić, Zoran S. Petrović, Tom Upshaw, Biobased Aromatic-Aliphatic Polyols from Cardanol by Thermal Thiol-Ene Reaction, *Journal of Renewable Materials*, 6, 1, (2018), 87-101 https://doi.org/10.7569/JRM.2017.634153

[18] Haoran Wang, Qixin Zhou, Synthesis of Cardanol-Based Polyols via Thiol-ene/Thiol-epoxy Dual Click-Reactions and Thermosetting Polyurethanes Therefrom, *ACS Sustainable Chemistry & Engineering*, 6, 9, (2018), 12088-12095 http://dx.doi.org/10.1021/acssuschemeng.8b02423

[19] Haniffudin Nurdiansah, Diah Susanti, Anni Rahmat, Fakhreza Abdul, Amaliya Rasyida, Hariyati Purwaningsih, Azzah Dyah Pramata, Retno Asih, Sintesis dan Karakterisasi Minyak *Cashew Nut Shell Liquid* (CNSL) dari Limbah Kulit Biji Mete Desa Blaru, Badas, Kediri dengan Metode Press Panas, *Sewagati*, 6, 6, (2022), 735-743 https://doi.org/10.12962/j26139960.v6i6.275

[20] Maria Yuliana, Bich Thuyen Nguyen-Thi, Sitti Faika, Lien Huong Huynh, Felycia Edi Soetaredjo, Yi-Hsu Ju, Separation and purification of cardol, cardanol and anacardic acid from cashew (*Anacardium occidentale* L.) nut-shell liquid using a simple two-step column chromatography, *Journal of the Taiwan Institute of Chemical Engineers*, 45, 5, (2014), 2187-2193 https://doi.org/10.1016/j.jtice.2014.07.012

[21] Natalia Toncheva-Moncheva, Miroslav Dangalov, Nikolay G. Vassilev, Christo P. Novakov, Thiol–ene coupling reaction achievement and monitoring by "*in situ*" UV irradiation NMR spectroscopy, *RSC Advances*, 10, 42, (2020), 25214-25222 http://dx.doi.org/10.1039/D0RA03902K

[22] Yang Zhang, Guangbin Song, Can Hu, Zixu Liu, Huansen Liu, Yilei Wang, Liang Wang, Xuequan Feng, Perfluoropolyether-incorporated polyurethane with enhanced antibacterial and anti-adhesive activities for combating catheter-induced infection, *RSC Advances*, 14, 1, (2024), 568-576 http://dx.doi.org/10.1039/D3RA07831K

[23] Kanyarat Mantala, Daniel Crespy, Waterborne Polyurethane Transparent Coatings for Self-Healing at Room Temperature, *Macromolecules*, 58, 7, (2025), 3450-3459 https://doi.org/10.1021/acs.macromol.4c02732

[24] John O. Akindoyo, M. D. H. Beg, Suriati Ghazali, M. R. Islam, Nitthiyah Jeyaratnam, A. R. Yuvaraj, Polyurethane types, synthesis and applications – a review, *RSC Advances*, 6, 115, (2016), 114453-114482 https://doi.org/10.1039/C6RA14525F

[25] Phasinee Khwanmuang, Chanita Naparswad, Somwit Archakunakorn, Chattaruk Waicharoen, Chayanisa Chitichotpanya, Optimization of in situ synthesis of Ag/PU nanocomposites using response surface methodology for self-disinfecting coatings, *Progress in Organic Coatings*, 110, (2017), 104-113 https://doi.org/10.1016/j.porgcoat.2017.03.002

[26] Karolina Fila, Beata Podkościelna, Maciej Podgórski, Cross-Linked Polythiomethacrylate Esters Based on Naphthalene—Synthesis, Properties and Reprocessing, *Materials*, 13, 13, (2020), 3021 https://doi.org/10.3390/ma13133021

[27] Wuting Pang, Hao Jiang, Shuai Wang, Tinglei He, Huang Chen, Tong Yan, Meng Cheng, Shuangqing Sun, Chunling Li, Graphene oxides enhanced polyurethane based composite coating with long term corrosion resistance and self-healing property, *European Polymer Journal*, 207, (2024), 112825 https://doi.org/10.1016/j.eurpolymj.2024.112825

[28] Bhavika Bhatia, Nagarjuna Amarnath, Sumit K. Rastogi, Bimlesh Lochab, Isolation of Cardanol Fractions from Cashew Nutshell Liquid (CNSL): A Sustainable Approach, *Sustainable Chemistry*, 5, 2, (2024), 68-80 https://doi.org/10.3390/suschem5020006

[29] P. Phani Kumar, R. Paramashivappa, P. J. Vithayathil, P. V. Subba Rao, A. Srinivasa Rao, Process for Isolation of Cardanol from Technical Cashew (*Anacardium occidentale* L.) Nut Shell Liquid, *Journal of Agricultural and Food Chemistry*, 50, 16, (2002), 4705-4708 https://doi.org/10.1021/jf020224w

[30] Indrajit Bramhecha, Javed Sheikh, Inherent mosquito repellent-cum-multifunctional polyurethane for multifunctional coating of cotton fabric, *Journal of Industrial and Engineering Chemistry*, 132, (2024), 247-258 https://doi.org/10.1016/j.jiec.2023.11.017

[31] Hongling Guo, Ping Wang, Can Hu, Hongcheng Mei, Yajun Li, Jun Zhu, Forensic comparison analysis of smokeless powders by gel permeation chromatography and likelihood ratio evaluation methods, *Forensic Sciences Research*, 10, 2, (2024), owaf005 https://doi.org/10.1093/fsr/owaf005

[32] Gopinath Kasi, Sathishkumar Gnanasekar, Kai Zhang, En Tang Kang, Li Qun Xu, Polyurethane-based composites with promising antibacterial properties, *Journal of Applied Polymer Science*, 139, 20, (2022), 52181 https://doi.org/10.1002/app.52181